On the Effect of DC Source Voltage on Inverter-Based Frequency and Voltage Regulation in a Military Microgrid

Tulga Ersal, Changsun Ahn, Ian A. Hiskens, Huei Peng, Anna Stefanopoulou, Jeffrey L. Stein

Abstract—**Increasing concerns about energy security and reliability are intensifying the military's interest in the microgrid technology. This paper focuses on the frequency and voltage regulation part of a case study that seeks to design a conceptual military microgrid that has to operate completely autonomously. This microgrid comprises a solar panel and vehicles as power sources, where the vehicles contain a battery and generator, and managing their power setpoints is the control problem of interest. The goal is to investigate the validity of assuming the battery as a constant voltage source during the control design. To this end, the control design is first carried out assuming the battery as a constant voltage source. It is then illustrated how critical this assumption can be depending on the battery internal resistance. The results show that the battery internal resistance can affect both frequency and voltage regulation performances, thereby highlighting the coupling between the battery characteristics and control design, and the need for a control design framework that takes this coupling into account.**

I. INTRODUCTION

MICROGRIDS are a collection of power loads and micro-sources functioning as a single system that can operate either in connection with a larger power grid or completely autonomously [1]. They have been attracting much research interest due to their potential to increase energy security and reliability, as well as foster the penetration of distributed renewable resources (e.g., wind, solar) and distributed storage (e.g., plug-in vehicles, community energy storage) [2-11]. Because of this potential, the U.S. Department of Defense (DoD) is interested in microgrids as indicated by the SPIDERS (Smart Power Infrastructure Demonstration for Energy Reliability and Security) project, which aims to demonstrate the first complete DoD installation with a secure microgrid capable of islanding.

Whereas the SPIDERS project presents an example microgrid that can operate in both grid-connected and islanded mode, forward operating bases (FOBs) – military bases temporarily established to support tactical operations – exemplify the need for maximizing operational autonomy.

Traditionally, these microgrids have relied entirely on diesel generators, whose transportation and fuel re-supply increase the vulnerability of the FOB. Indeed, electric power generation can account for over 70% of fuel consumption at or near the tactical edge [12], and the U.S. Army indicates that 50% of the casualties during resupply missions in Iraq and Afghanistan are due to fuel delivery [13].

To make FOBs more sustainable, the microgrid can leverage local renewable resources and military vehicles with on-board electrical generation and energy storage capability. Such a concept FOB considered in this paper is shown in Fig. 1. Instead of relying entirely on stationary generators, it integrates into the microgrid a solar panel and numerous vehicles with a battery and generator. Note that electric equipment such as radars, radios, and computers require significant on-board electric generation and storage in military vehicles to reduce idling of the main propulsion engine and for silent watch.

Two types of the sources in the example microgrid, namely, the solar panel and the battery, are DC and need an inverter interface to connect them to an AC microgrid (e.g., see Fig. 2). Controlling the inverter is critical to regulate AC voltage and power, as well as to establish frequency during autonomous operation [14]. Many techniques have been proposed and used to achieve this goal [6, 10, 11, 14-16]. Such techniques typically assume that the DC voltage supplied to the inverter remains constant. However, DC sources such as batteries exhibit voltage variations depending on the power drawn from them. Thus, even though assuming such sources as constant voltage supplies could greatly simplify the control design problem, it is
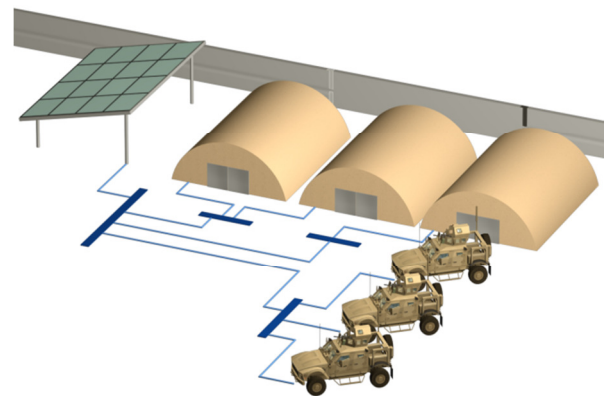

Fig. 1. Example conceptual military microgrid considered in this study for a forward operating base (FOB). The power sources consist of a solar panel and electrified vehicles.
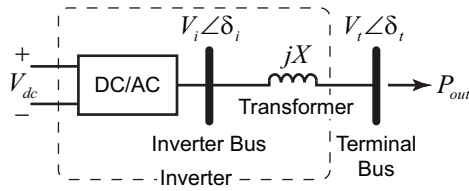
Fig. 2. Inverter-grid interface model.

Fig. 4.Electricity grid model of the example microgrid shown in Fig. 1.

necessary to understand the consequences of this assumption. Hence, the goal of this paper is to examine the validity of this assumption for the example microgrid shown in Fig. 1.

With this goal in mind, the paper first develops a model for the example microgrid. A fixed-structure controller is proposed to manage the power setpoints of the battery and generator. The controller is designed with the assumption that the battery is a constant voltage source. Then, the battery is modeled as a voltage source in series with a resistor to approximate the battery internal resistance and its power limitation. With this simple electrical model, the effect of the battery resistance, or power availability, on frequency and voltage regulation is investigated.

The microgrid operating condition considered in this paper is based on the worst-case scenario from a higher-level design and scheduling study that optimized the sizes of the solar panel, batteries, and generators, as well as the power dispatch over a period of one year using a forward-looking strategy to minimize annualized capital and fuel costs. The mathematical formulation of this nested design and dispatch optimization is given in detail in [17]. The FOB was sized for 50 soldiers, using 120 kW peak power and 67 kW average power. Solar radiation data from Afghanistan was used. The optimization resulted in a solar panel of 89 kW, a total of 8.4 kWh battery capacity, and a total of 120 kW generator power. The worst-case scenario was defined as the maximum difference between generated and used power. Fig. 3 illustrates the hourly load and generation trajectories for all the components in the microgrid for one of the days on which an abrupt and large transient, in fact, one of the
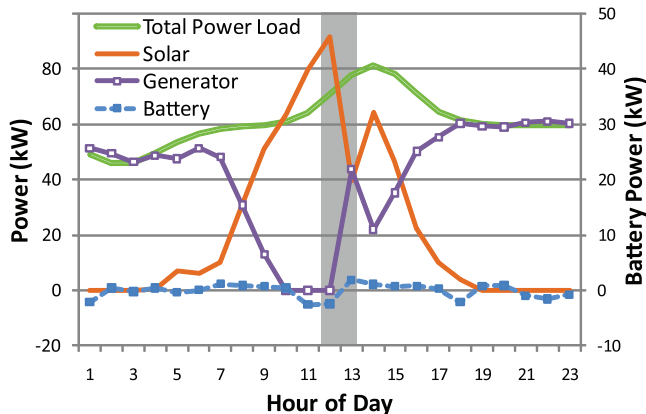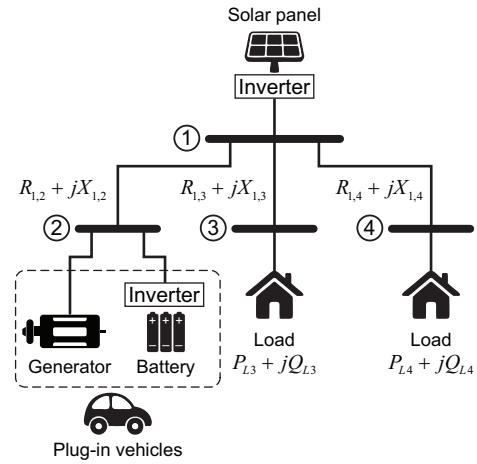
worst-case transients, occurred. The worst-case is shown in the shaded region. It corresponds to an instant when there is initially enough solar power to supply the loads and charge the batteries, and hence the generators are idling. A 50kW drop then occurs in the solar power, and the batteries and generators must be controlled to support the loads and stabilize the microgrid. As can be seen in Fig. 3 the optimum and forward-looking hourly sequence of commands involves the simultaneous increase of the battery and the generator power. For the purposes of this paper, it will be assumed that a drop of this magnitude could happen instantaneously and unexpectedly.

II. MODELING AND CONTROL

A. Modeling the Microgrid

The microgrid in Fig. 1 consists of four buses: Two of them are connected to loads; one is connected to an intermittent power source, namely, the solar panel; and one is connected to a reconfigurable energy storage and power source, namely, a group of vehicles. The grid is modeled as shown in Fig. 4. For the purposes of this paper, the vehicles are aggregated into a single generator and battery that are controlled independently. The vehicles are assumed to be always available for supporting the microgrid. Furthermore, within the short time scale of interest (i.e., seconds), the number of vehicles connected to the microgrid is assumed to remain constant, leading to a constant generator and battery size. The loads are assumed critical and hence no load-side power management (e.g., load shedding) is considered in this paper.

The solar panel and battery are interfaced with the AC microgrid through inverters. A model for the inverter-grid interface is shown in Fig. 2. The inverter is controlled to regulate the voltage V_t at the terminal bus and active power output P_{out} to the grid. This is achieved by controlling the modulation index m of the inverter, which effectively controls the inverter voltage magnitude V_i through the relationship

Fig. 3. The power profiles for the day that contains the worst case scenario considered in this paper (the shaded region).

$$V_i = m \frac{V_{dc}}{V_{base}}, \tag{1}$$

and the inverter firing angle, which effectively determines the phase angle δ_i. In (1), V_{base} is the base unit voltage that is used for normalization to allow working with the per-unit system [18], and V_{dc} is the DC voltage supplied to the inverter by the DC power source.

This paper considers a phase-locked loop (PLL) based inverter control strategy as proposed by Hiskens and Fleming [14]. The PLL is needed to estimate the phase difference between the inverter and terminal AC voltage waveforms [19], which is then controlled to regulate the power delivered to the microgrid. The dynamics of the inverter controller are given by the following set of differential-algebraic equations:

$$\dot{m} = K_1 \left(V_{set} - V_t \right), \tag{2a}$$

$$\dot{\theta} = K_2 \left(P_{set} - P_{out} \right), \tag{2b}$$

$$\dot{x} = K_3 \left(\delta_t - \delta_p \right), \tag{2c}$$

$$\dot{\delta}_p = \omega_p, \tag{2d}$$

$$0 = V_i - \frac{m V_{dc}}{V_{base}}, \tag{2e}$$

$$0 = \theta - \left(\delta_i - \delta_p \right), \tag{2f}$$

$$0 = x - \left(\omega_p - K_4 \theta \right), \tag{2g}$$

$$0 = P_{out} - \frac{V_i V_t}{X} \sin \left(\delta_i - \delta_t \right). \tag{2h}$$

(2a) and (2b) correspond to integral control of V_t and P_{out}, where V_{set} and P_{set} are the set values for V_t and P_{out}, respectively. (2c) and (2d) describe the PLL dynamics, which, in addition to integral control, also involves damping due to the term $K_4 \theta$ in the definition of the variable x. The variable δ_p represents the PLL phase angle, and its time derivative, ω_p provides an estimate of the deviation of
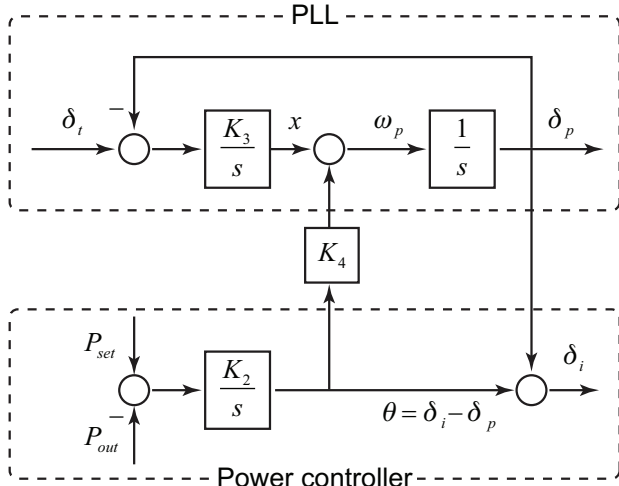

Fig. 5. The power control scheme used in this paper.

system frequency from nominal. (2f) and (2g) define the variables θ and x, respectively. Finally, (2h) gives the active power delivered to the grid. The block diagram shown in Fig. 5 illustrates the interaction between the PLL and the power control scheme.

In this study, (2) is used to model the inverters for both the solar panel and the battery. In addition to (2), the equations for the solar panel inverter are augmented with the following exogenous input for the power setpoint

$$P_{set} = P_{solar} \left(t \right), \tag{3}$$

where $P_{solar} \left(t \right)$ is the available solar power at time t.

Without any control over the loads and solar panel setpoint, the only components to be considered in the power setpoint control problem are the vehicle battery and generator. This is addressed in Section II.C.

Finally, the power balance in the buses is modeled as follows. Using the phasor notation, the terminal voltages are given by

$$\mathbf{V}_{tn} = V_{tn} e^{j\delta_{tn}}, \quad n = 1, 2, 3, 4, \tag{4}$$

where n is an index for the terminals. The line impedances between the terminals are expressed as

$$\mathbf{Z}_{1,n} = R_{1,n} + j X_{1,n}, \quad n = 2, 3, 4. \tag{5}$$

The line and inverter currents are thus obtained as

$$\mathbf{I}_{1,n} = \frac{\mathbf{V}_{t1} - \mathbf{V}_{tn}}{\mathbf{Z}_{1,n}}, \quad n = 2, 3, 4,$$

$$\mathbf{I}_{inv1} = \frac{\mathbf{V}_{i1} - \mathbf{V}_{t1}}{jX}, \quad \mathbf{I}_{inv2} = \frac{\mathbf{V}_{i2} - \mathbf{V}_{t2}}{jX} \tag{6}$$

The power balance equations are then

$$\mathbf{I}_{inv1} - \mathbf{I}_{1,2} - \mathbf{I}_{1,3} - \mathbf{I}_{1,4} = 0$$

$$\mathbf{V}_{t2} \left(\mathbf{I}_{1,2}^* + \mathbf{I}_{inv2}^* \right) + \left(P_{gen} + j Q_{gen} \right) = 0$$

$$\mathbf{V}_{t3} \mathbf{I}_{1,3}^* - \left(P_{L3} + j Q_{L3} \right) = 0 \tag{7}$$

$$\mathbf{V}_{t4} \mathbf{I}_{1,4}^* - \left(P_{L4} + j Q_{L4} \right) = 0$$

where asterisk denotes complex conjugate.

B. Modeling the Power Sources and Loads

The drop in solar power (due to weather, malfunction, attack, etc.) is assumed to happen instantaneously and is thus modeled as a step change as described by

$$P_{solar} \left(t \right) = \begin{cases} P_{solar}^1 & t \le t_1 \\ P_{solar}^2 & t > t_1 \end{cases} . \tag{8}$$

The generator is assumed to have first order dynamics as given by

$$P_{gen} \left(s \right) = \frac{1}{\tau_{gen} s + 1} P_{set}^{gen} \left(s \right). \tag{9}$$

TABLE I
MODEL PARAMETERS

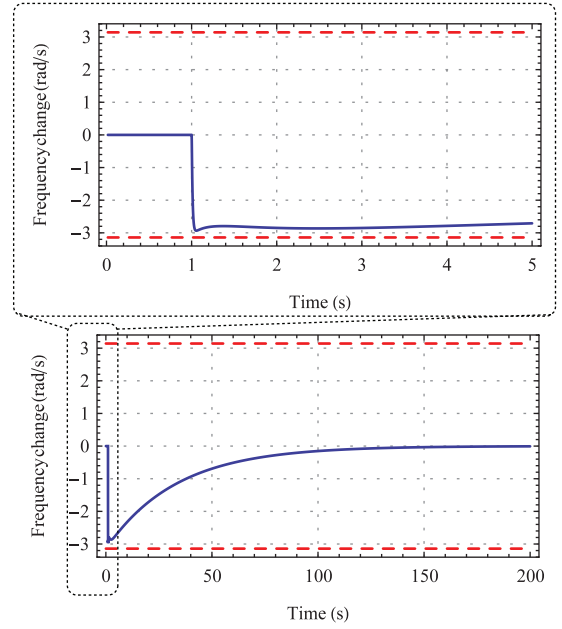| Parameter	Value	Parameter	Value
K_1	10	$R_{1,2}, R_{1,3}, R_{1,4}$	0.008 pu
K_2	20	$X_{1,2}, X_{1,3}, X_{1,4}$	0.004 pu
K_3	20	P_{solar}^1	7.949 pu
K_4	10 1/s	P_{solar}^2	2.97 pu
X	0.05 pu	P_{base}	10 kVA
V_{set}	1 pu	V_{base}	110 V
P_{L3}	3 pu	$V_{\text{dc}}^{\text{solar}}, V_{\text{OCV}}$	480 V
P_{L4}	3.42 pu	k_{1P}	0.086
Q_{L3}, Q_{L4}	0	k_{1a}	1.6016
$P_{\text{max}}^{\text{gen}}$	12 pu	k_{1I}	0.143
$P_{\text{op}}^{\text{gen}}, Q_{\text{gen}}$	0	k_{2P}	1.8
τ_{gen}	1 s	t_1	1 s
$P_{\text{op}}^{\text{batt}}$	-1.285 pu		

Fig. 6. Frequency regulation performance of the design assuming battery is a constant voltage source. Dashed lines represent the maximum allowed deviation limits.

The battery is modeled as a voltage source with an internal resistance. Within the time scale of interest (i.e., seconds), the change in the state-of-charge (SoC) is assumed to be negligible, and thus the SoC dependence of the open-circuit voltage (OCV) of the battery is neglected along with any other battery dynamics. We assume a string of batteries in series so that the nominal V_{OCV} at 50% charge is equal to the nominal bus voltage. As a result, the battery is represented using the following relationship:

$$V_{\text{dc}}^{\text{batt}} = V_{\text{OCV}} - R_{\text{batt}}I, \qquad (10)$$

where I is conserved positive when it discharges the battery.

Finally, the loads are assumed to be constant.

C. Control Structure

Within the considered framework, the only components whose power setpoints need to be managed are the vehicle battery and generator. The following feedback forms are proposed:

$$\begin{aligned}
P_{\text{set}}^{\text{gen}} &= -k_{1P}\omega_p - k_{1a}P_{\text{gen}} - k_{1I}\int \omega_p dt + P_{\text{op}}^{\text{gen}}, \\
P_{\text{set}}^{\text{batt}} &= -k_{2P}\omega_p + P_{\text{op}}^{\text{batt}}.
\end{aligned} \qquad (11)$$

where P_{op} represents the pre-disturbance operating point.

Note that the first terms on the right hand side of the equations correspond to the traditional droop control scheme [1, 6, 20-23]. The second term in the generator controller adds an additional feedback from the actual power output. This helps delay the engagement of the generator. A disturbance will then initially be compensated for mainly by the battery, helping save fuel. However, the battery cannot compensate for a large disturbance indefinitely due to its limited energy capacity. Hence, the generator controller also includes an integral action, so that any disturbance is ultimately compensated for entirely by the generator. This
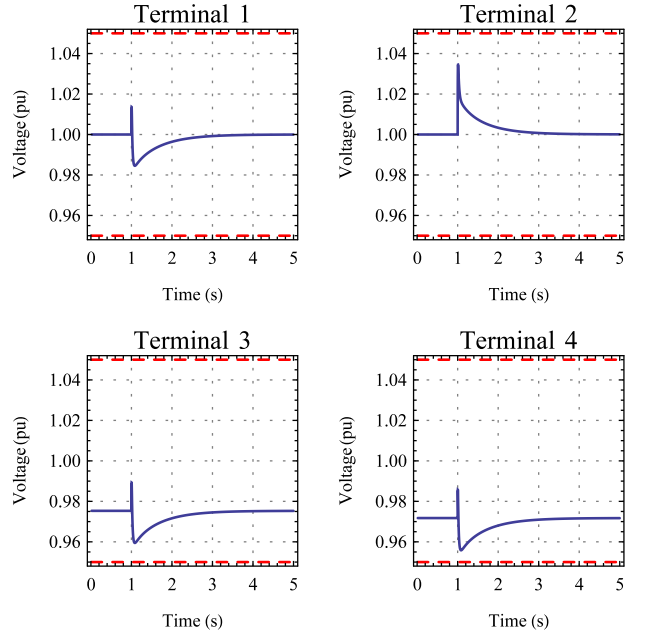

Fig. 7. Voltage regulation performance of the design for all the terminals assuming battery is a constant voltage source. Dashed lines represent the maximum allowed deviation limits.

control scheme ensures that in the post-disturbance steady state the frequency deviation is zero, thereby enabling the battery to return to its original operating condition, whereas the generator power output settles to $-k_{1a}P_{gen} - k_{1I}\int \omega_p dt + P_{\text{op}}^{\text{gen}}$. It is assumed that a higher-level dispatch controller exists that will eventually be informed about the disturbance and will determine the new (optimal) operating conditions for the generator and battery.
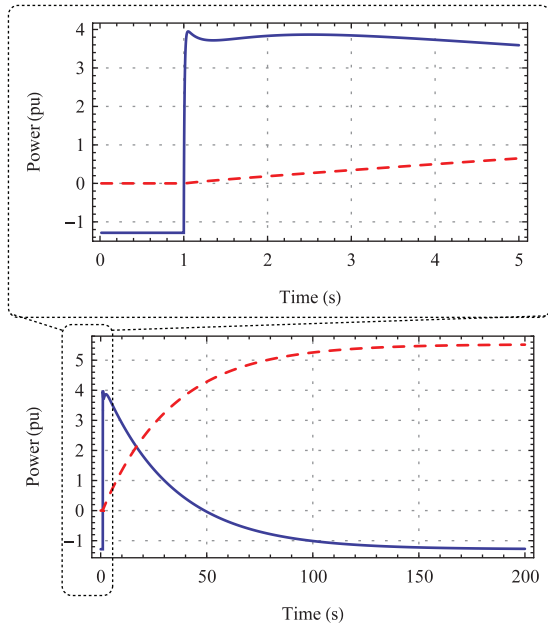
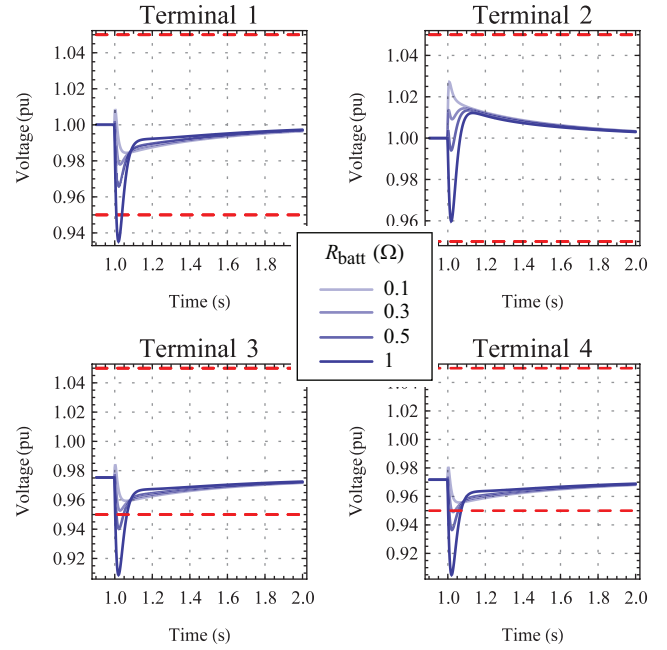Fig. 8. Battery (solid) and generator (dashed) power.

Fig. 9. Terminal voltage regulation performance of the controller for various battery internal resistance values. Dashed lines represent the maximum allowed deviation limits.
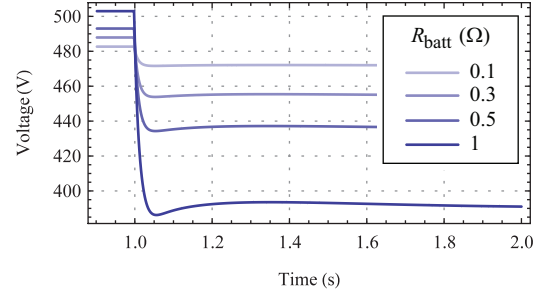

Fig. 10. Battery voltage trajectories for various battery internal resistance values.

Also note the decentralized character of the controllers in (11). The only common signal to the controllers is the frequency deviation ω_p; the controllers are otherwise independent, use only the locally available information (i.e., frequency and local power), and do not require any communication with each other or any other component in the microgrid.

III. SIMULATION RESULTS AND DISCUSSION

The microgrid system described above is simulated and optimized for the parameter values given in Table I. The parameter values for the inverter grid interface and inverter control gains are taken from [14]. The loads, step change in solar power, and the operating points for the battery and generator are obtained from a worst-case scenario of the design and scheduling study. The maximum allowed frequency and voltage deviations were set to 0.5 Hz and 5%, respectively. The control gains were tuned by linearizing the model around the given operating point and numerically solving an LQR problem with power and frequency constraints, as well as the constraint that the battery has to return to its original state within 200 s to avoid draining the battery with subsequent energy extractions. During the control design, the battery internal resistance was neglected and the battery was assumed to be a constant voltage source. Hence, voltage constraints were also neglected in the constrained LQR formulation. The objective was to minimize the frequency deviation, as well as the power drawn from the generator. The constraints were included with a large penalty in the optimization problem formulation, and the resulting problem was solved with an unconstrained nonlinear programming solver. The remaining parameters were assumed.

Fig. 6 and 7 show the frequency and voltage regulation performance of the controller. In these figures, the nonlinear microgrid model was used; however, the battery voltage was assumed to be constant to show the nominal performance of the controller. As the figures illustrate, both the frequency and voltage can be regulated successfully within the desired limits, if the battery voltage remains constant.

Fig. 8 shows the battery and generator power trajectories during the disturbance. Initially, the microgrid is stabilized using mainly the battery. Gradually, the generator power is increased, and, due to the integral action in the generator control scheme in (11), the generator completely compensates for the power loss in the post-disturbance steady state, allowing the battery to return to its original charging state.

To check the effects of the violation of the constant battery voltage assumption on the performance, the simulation is repeated including the battery internal resistance and varying it from 0.1 to 1 Ω with 0.1 Ω increments. Fig. 9 shows the voltage regulation performance of the controller for various values of R_{batt}. Voltage constraint violation begins for $R_{batt} = 0.3\,\Omega$ at terminal 4.

Violations at other terminals are also observed for higher values of R_{batt}. The corresponding battery voltages are shown in Fig. 10.

The frequency regulation performance is not affected significantly for the range of R_{batt} values considered and thus the corresponding plot is not shown. To understand the physical reason behind the high sensitivity of voltage regulation performance and low sensitivity of the frequency regulation performance, first recall that frequency is closely related to the power balance in the system; an excess power generation will increase the frequency, whereas power deficiency will result in a frequency drop. Thus, a given frequency drop can be initially compensated only with a commensurate power draw from the battery. When the battery internal resistance increases, the same power draw can be achieved only at the expense of a higher current, which in turn results in a lower battery voltage. Battery voltage, however, is critical for the inverter to regulate the terminal voltage. Thus, the voltage regulation performance may suffer, if the system is designed only with frequency (i.e., power) considerations. On the other hand, the battery
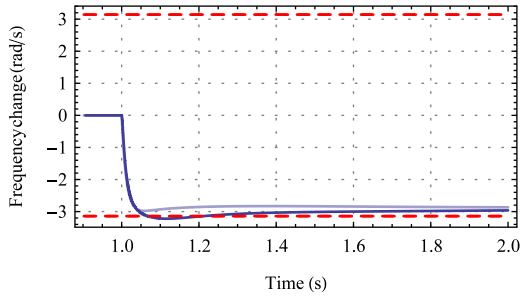

Fig. 11. Frequency regulation performance for $R_{batt} = 1\,\Omega$ and $K_1 = 10$ (light) versus $K_1 = 200$ (dark).
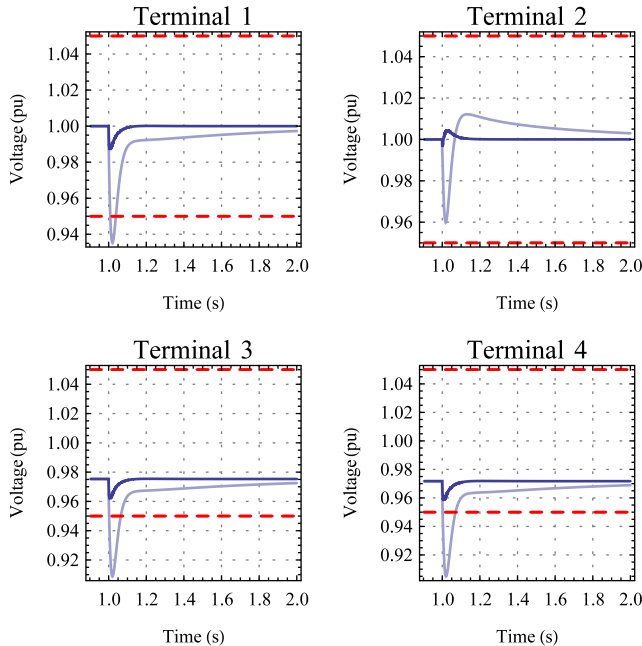

Fig. 12. Voltage regulation performance for $R_{batt} = 1\,\Omega$ and $K_1 = 10$ (light) versus $K_1 = 200$ (dark).
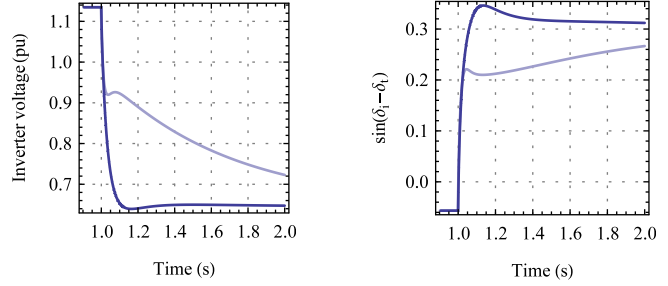

Fig. 13. Battery Inverter voltage (left) and the phase difference between battery inverter and terminal for $K_1 = 10$ (light) versus $K_1 = 200$ (dark).

power needed to stabilize the frequency in the considered scenario is around 40 kW (Fig. 8), whereas the maximum theoretical battery power available when $R_{batt} = 1\,\Omega$ is

$$P_{max}^{batt} = \frac{V_{OCV}^2}{4R_{batt}} = 57.6 \text{ kW}$$

Hence, the battery is still capable of providing the power needed, but at a lower voltage than what is necessary to keep the terminal voltages within desired limits.

The high and low sensitivities of voltage and frequency regulation performances to the battery voltage fluctuations may seem to indicate that the voltage and frequency regulation problems are decoupled and hence the voltage control gain K_1 of the inverters may be increased to reduce the sensitivity of the voltages without affecting the frequency regulation performance. Fig. 11 and 12 illustrate, however, that this is not necessarily true. These figures compare the regulation performances for the original value of $K_1 = 10$ and for $K_1 = 200$. In both cases R_{batt} was set to 1 Ω. Higher controller gain greatly improves the voltage regulation performance to the degree that all terminal voltages are well within the desired limits. However, the frequency constraint is violated. This is because a higher value for K_1 increases the sensitivity of the inverter AC voltage to the battery DC voltage, see (2a) and (2e). This implies that the drop in the DC voltage is more strongly reflected in the inverter AC voltage (Fig. 13). As a result, $V_i V_t / X$ term in the AC power delivered to the grid (see (2g)) decreases and a higher phase difference $\delta_i - \delta_t$ becomes necessary to balance frequency. Achieving the needed phase difference takes more time (Fig. 13), and during that time the frequency falls below the allowed limit.

Therefore, it is critical to consider the voltage-current characteristics of the battery carefully and compensate for undesired voltage drops either in the control design (e.g., by taking the battery characteristics into account and considering both frequency and voltage regulation together), or in the battery design (e.g., by changing battery chemistry, increasing battery size, adding capacitors in parallel, etc.).

IV. SUMMARY AND CONCLUSION

This paper considered a conceptual military microgrid that operates completely autonomously, i.e., without a connection to a larger power grid. A solar panel, vehicle batteries and generators were assumed to be the power sources, whereas loads were assumed to be constant and uncontrollable. Leveraging a phase-locked loop based inverter control strategy from the literature, this paper considered a power setpoint control algorithm for the batteries and generators. The controller was tuned assuming the battery voltage is constant. The impact of this assumption was then tested by considering a range of values for the battery internal resistance. The results showed that the battery internal resistance can affect both frequency and voltage regulation performances. Thus, an effective inverter-based control design framework should consider both regulation problems together, as well as the voltage-current characteristics of the DC sources.

REFERENCES

[1] R. Lasseter, A. Akhil, C. Marnay, J. Stephens, J. Dagle, R. Guttromson, A. S. Meliopoulous, R. Yinger, and J. Eto, "Integration of distributed energy resources: The CERTS microgrid concept," U.S. Department of Energy and California Energy Commission, LBNL-50829, 2002.

[2] H.-w. Zhao and T.-t. Wu, "Review of distributed generation based microgrid technology," Proceedings of the CSU-EPSA, vol. 20, no. 1, pp. 121-8, 2008.

[3] M. A. Sofla and G. B. Gharehpetian, "Dynamic performance enhancement of microgrids by advanced sliding mode controller," International Journal of Electrical Power and Energy Systems, vol. 33, no. 1, pp. 1-7.

[4] D. Pudjianto, C. Ramsay, and G. Strbac, "Microgrids and virtual power plants: Concepts to support the integration of distributed energy resources," Proceedings of the Institution of Mechanical Engineers, Part A: Journal of Power and Energy, vol. 222, no. 7, pp. 731-741, 2008.

[5] J. A. P. Lopes, S. A. Polenz, C. L. Moreira, and R. Cherkaoui, "Identification of control and management strategies for LV unbalanced microgrids with plugged-in electric vehicles," Electric Power Systems Research, vol. 80, no. 8, pp. 898-906, 2010.

[6] J. A. P. Lopes, C. L. Moreira, and A. G. Madureira, "Defining control strategies for microgrids islanded operation," IEEE Transactions on Power Systems, vol. 21, no. 2, pp. 916-924, 2006.

[7] T. Logenthiran, D. Srinivasan, and A. M. Khambadkone, "Multi-agent system for energy resource scheduling of integrated microgrids in a distributed system," Electric Power Systems Research, vol. 81, no. 1, pp. 138-148.

[8] N. W. A. Lidula and A. D. Rajapakse, "Microgrids research: A review of experimental microgrids and test systems," Renewable and Sustainable Energy Reviews, vol. 15, no. 1, pp. 186-202.

[9] N. Jayawarna and M. Barnes, "Study of a microgrid with vehicle-to-grid sources during network contingencies," Intelligent Automation and Soft Computing, vol. 16, no. 2, pp. 289-302, 2010.

[10] J. M. Guerrero, J. Matas, L. G. De Vicuna, M. Castilla, and J. Miret, "Wireless-control strategy for parallel operation of distributed-generation inverters," IEEE Transactions on Industrial Electronics, vol. 53, no. Compendex, pp. 1461-1470, 2006.

[11] T. C. Green and M. Prodanovic, "Control of inverter-based micro-grids," Electric Power Systems Research, vol. 77, no. Compendex, pp. 1204-1213, 2007.

[12] DARPA, "Darpa-BAA-11-53: Deployed energy storage," S. T. O. (STO), Ed., 2011.

[13] D. S. Eady, S. B. Siegel, R. S. Bell, and S. H. Dicke, "Sustain the mission project: Casualty factors for fuel and water resupply convoys," Army Environmental Policy Institute, Final Technical Report, NSN 7540-01-280-5500, 2009.

[14] I. A. Hiskens and E. M. Fleming, "Control of inverter-connected sources in autonomous microgrids," 2008 American Control Conference, pp. 586-590, IEEE, 2008.

[15] K. De Brabandere, B. Bolsens, J. Van den Keybus, A. Woyte, J. Driesen, and R. Belmans, "A voltage and frequency droop control method for parallel inverters," IEEE Transactions on Power Electronics, vol. 22, no. Compendex, pp. 1107-1115, 2007.

[16] T. Ersal, C. Ahn, I. A. Hiskens, H. Peng, and J. L. Stein, "Impact of controlled plug-in EVs on microgrids: A military microgrid example," IEEE Power & Energy Society General Meeting, Detroit, MI USA, 2011.

[17] J. Whitefoot, A. Mechtenberg, D. Peters, and P. Papalambros, "Optimal component sizing and forward-looking dispatch of an electrical microgrid for energy storage planning," ASME International Design Engineering Technical Conferences & Computers and Information in Engineering Conference (IDETC/CIE), 2011.

[18] J. D. Glover, M. S. Sarma, and T. J. Overbye, Power system analysis and design Thomson, 2008.

[19] D. Abramovitch, "Phase-locked loops: A control centric tutorial," American Control Conference, Anchorage, AK, USA, vol. 1, pp. 1-15, IEEE, 2002.

[20] J. A. P. Lopes, C. C. L. Moreira, and F. O. Resende, "Microgrids black start and islanded operation," 15th Power Systems Computation Conference, Liege, Belgium 2005.

[21] N. J. Gil and P. A. Lopes, "Hierarchical frequency control scheme for islanded multi-microgrids operation," 2007 IEEE Lausanne POWERTECH, pp. 473-478, Institute of Electrical and Electronics Engineers Computer Society, 2007.

[22] R. H. Lasseter and P. Paigi, "Microgrid: A conceptual solution," 2004 IEEE 35th Annual Power Electronics Specialists Conference, vol. 6, pp. 4285-4290, Institute of Electrical and Electronics Engineers Inc., 2004.

[23] R. H. Lasseter, "CERTS microgrid," 2007 IEEE International Conference on System of Systems Engineering, Inst. of Elec. and Elec. Eng. Computer Society, 2007.